Title

An acidic microenvironment produced by the V-type ATPase of Euprymna scolopes promotes specificity during Vibrio fischeri recruitment.

Journal

Communications Biology, 7(1)

Authors

Hargadon, Alexis

Viliunas, Joani

Koehler, Sabrina

et al.

Publication Date

2024-12-18

DOI

10.1038/s42003-024-07348-2

Peer reviewed

communications biology

Article

https://doi.org/10.1038/s42003-024-07348-2

An acidic microenvironment produced by the V-type ATPase of *Euprymna scolopes* promotes specificity during *Vibrio fischeri* recruitment

Check for updates

Alexis C. Hargadon[1,5], Joani W. Viliunas[1,2,5], Sabrina Koehler[3], Angus B. Thies[4], Grischa Y. Chen[1], Mark S. Ladinsky[2], Jill Kuwabara[1], Viridiana Avila-Magana[1], Edward G. Ruby[2], Martin Tresguerres[4] & Margaret J. McFall-Ngai[1,2]

Animals often acquire their microbial symbionts from the environment, but the mechanisms underlying how specificity of the association is achieved are poorly understood. We demonstrate that the conserved proton pump, V-type ATPase (VHA), plays a key role in the establishment of the model light-organ symbiosis between the squid *Euprymna scolopes* and its bacterial partner, *Vibrio fischeri*. Recruitment of *V. fischeri* from the surrounding seawater is mediated by juvenile-specific ciliated fields on the organ's surface. These epithelia produce acidic mucus containing antimicrobials with low-pH optima, creating a chemical environment fostering specific recruitment of *V. fischeri*. We provide evidence that this critical acidic landscape is created by activity of VHA. VHA inhibition abolished epithelial-cell acidity, resulting in increased mucus pH and inefficient symbiont colonization. Thus, VHA provides a mechanistic link between host modulation of microenvironmental acidity, immune function, and selection of microbial symbionts, a strategy for specificity that may govern other symbioses.

Many invertebrates and most, if not all, vertebrates acquire their bacterial symbionts by horizontal transmission, i.e., the symbionts are not present during embryogenesis, but are recruited from the environment during or after birth or hatching[1]. Nonetheless, the embryonic period can prepare the cells and tissues of the host animal to recognize their proper microbial partners [see, e.g.[2,3],]. The process of symbiont recruitment in terrestrial environments is well understood, as it is typically facilitated by direct interactions with conspecifics (e.g., parents and/or nest mates[4–6]). In contrast, horizontally transmitted symbionts in aquatic environments select their often-rare partners against a rich background of nonspecific microbes in the surrounding water, and the precise mechanisms fostering this challenge of recruitment remain poorly understood.

The model symbiosis between the Hawaiian bobtail squid *Euprymna scolopes* and its luminescent bacterial partner *Vibrio fischeri* offers the opportunity to study the underlying mechanisms of the symbiont-acquisition process in the marine environment [for review, see ref. 7]. Notably, this system has temporal and physical features associated with symbiont recruitment that allow detailed biochemical and microscopic analyses of this process. Embryogenesis prepares the ~2-mm newly hatched juvenile animal for recruitment of its proper symbiont. Specifically, the nascent symbiotic light-emitting organ (Fig. 1) develops juvenile-specific ciliated fields that, following hatching, facilitate the enrichment of *V. fischeri* cells in small aggregates above a series of pores on the organ surface. These pores lead to migration paths ending at crypts that will be the sites of *V. fischeri* residence over the life of the squid. The colonization process occurs within hours and across a short (~150 μm), but biochemically and biomechanically complex, migration path. *E. scolopes*, a night-active predator in the shallow backreefs of the Hawaiian archipelago, emits symbiont-produced luminescence from its ventral surface, presumably as an anti-predatory strategy[8].

Studies of the first several hours of this host-symbiont interaction have demonstrated that a complex dialogue between the partners is required for a

[1]Division of Biosphere Sciences and Engineering, Carnegie Science, Pasadena, CA, USA. [2]Division of Biology and Biological Engineering, California Institute of Technology, Pasadena, CA, USA. [3]Evolutionary Ecology and Genetics, Zoological Institute, Kiel University, Kiel, Germany. [4]Marine Biology Research Division, Scripps Institution of Oceanography, University of California, San Diego, La Jolla, CA, USA. [5]These authors contributed equally: Alexis C. Hargadon, Joani W. Viliunas. e-mail: mcfallng@caltech.edu

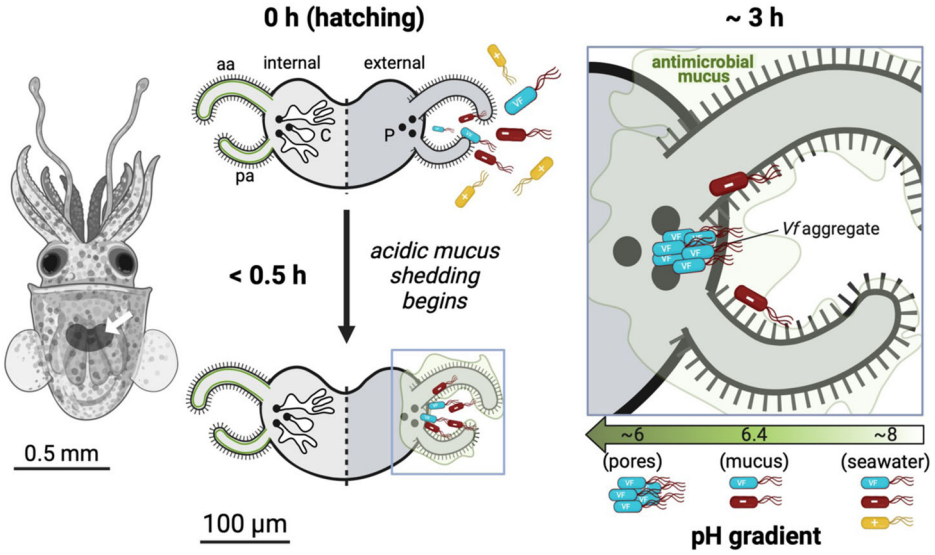

Fig. 1 | Features of the juvenile *E. scolopes* light organ that foster recruitment of environmental *V. fischeri* cells. *Left*, diagram of a ventral view of a hatchling squid showing the internal organ's position in the center of the mantle cavity (white arrow). *Middle*, diagrams of the internal and external features of the juvenile organ, before and after mucus shedding in response to environmental peptidoglycan; aa/pa, anterior/posterior appendages on the organ surface; P, pores near which environmental bacteria aggregate before migrating into and colonizing the deep crypts, C. Bacteria in the ambient seawater include *V. fischeri* (VF; blue), and other gram negative ('-'; red) or gram positive ('+'; yellow) cells. *Right*, zoomed in diagram of one side of the organ surface, showing the gradient of acidification that develops in the mucus during the first hours following hatching. This acidification, together with an array of antimicrobial proteins and peptides in the mucus, select against cells that are not *V. fischeri*. The resulting biochemical and biomechanical environment created near the pores fosters the dominance of *V. fischeri* cells in the aggregates within ~3 h of hatching. Modified from images created by BioRender.

successful association to ensue[7,9]. Briefly, within a few minutes, the superficial ciliated fields on the light organ shed copious amounts of mucus in a non-specific response to cell-wall (i.e., peptidoglycan) derivatives produced by the ambient bacterioplankton. From the more distant edges of the ciliated fields to the region of the pores, a pH gradient develops[10], ranging from ~8.1 (the pH of seawater) to ~6.4 in the mucus, and ~5.9 at the pores (Fig. 1, right). Within this mucus matrix is a dilute cocktail of 10–12 antimicrobials that have been shed from the apical surfaces of the ciliated epithelia and whose activities have pH optima under acidic conditions, a characteristic of most antimicrobial proteins and peptides[11]. Once in the crypts, the population of symbionts proliferates, filling the spaces by about 12 h after the initial exposure to planktonic *V. fischeri* cells. At this point, bacterial cell-envelope products induce the gradual loss over 4-5 d of the superficial ciliated epithelial fields that potentiate recruitment; in addition, sometime between 12 and 24 h, mucus shedding from the ciliated fields ceases[12].

In a complex process occurring during the first several hours, selection of the specific symbiont occurs on the organ surface. Although in the absence of *V. fischeri* cells other Gram-negative bacteria will aggregate along the cilia, if symbiont-competent strains of *V. fischeri* are present, they will outcompete the other members of the bacterioplankton[13]. Studies of *V. fischeri* have provided evidence that a host-created biochemical 'cocktail' produces conditions that prime *V. fischeri* for the journey to the crypts via the migration paths, which have high concentrations of antimicrobials (for review, see ref. 9). The *V. fischeri* cells that aggregate on the surface attach to the host's ciliated epithelial cells, causing further upregulation of genes encoding the antimicrobials and their export into the mucus[10]. Nanoscale secondary ion mass spectrometry (NanoSIMS) studies have shown that all *V. fischeri* cells in the migration paths are living, whereas other bacterial cells show evidence of antimicrobial melanization typical of dead or dying cells[14] and, in the absence of *V. fischeri*, the light organ remains uncolonized.

Previous studies have demonstrated that the selection of *V. fischeri* first occurs in the mucus matrix on the surface of the light organ's tissues; in particular, the data suggest that pH plays an important role in shaping the environment for successful acquisition of this highly specific symbiont. However, the mechanisms underlying the production of the acidic mucus-rich environment have not been explored. One promising candidate for this process is the vacuolar-type H^+ ATPase (VHA). This multiprotein, proton-pumping, membrane holoenzyme is ubiquitously present in eukaryotes[15,16] and, along with carbonic anhydrase (CA) and other proton-translocating proteins[17], is responsible for the acidification of intracellular compartments including the endoplasmic reticulum, the Golgi complex, endosomes, phagosomes, lysosomes, and melanosomes[18,19].

In vertebrate animals, VHA is also essential for the extracellular secretion of H^+ across several types of epithelia including those in kidney, epididymis, olfactory mucosa, inner ear, and lung[20]. Notably, VHA activity determines the acidic pH and high viscosity of the mucus-containing surface liquid that lines the mammalian airway epithelia and interacts with the associated microbiota[21]. For instance, VHA has been implicated in protecting vertebrate epithelia from pathogenic infection[22,23]; this function has not yet been well documented in invertebrates, although it may occur[24]. Among invertebrate animals, VHA ubiquitously drives the acidification of extracellular compartments including gut tracks[25,26] and extracellular protein matrices[27–30]. Furthermore, VHA has been recently shown to acidify the microenvironment surrounding algal symbionts of diverse marine invertebrate species[31–33]. Thus, VHA-dependent microenvironmental acidification may be an evolutionarily conserved mechanism used by invertebrate hosts to modulate the physiology of their symbiotic microbes.

In this study, we aimed to characterize VHA in juvenile *E. scolopes* and to determine the role of this protein in symbiont recruitment. Our studies of VHA in the juvenile light organ provide evidence that this protein is a critical player during the initiation of a successful life-long partnership between the squid host and its luminous bacterial partner.

Results and discussion

The enzyme VHA occurs in a wide array of epithelial tissues of *E. scolopes*, and its phylogeny and molecular structure are consistent with expected patterns

We identified VHA subunits encoded in the *E. scolopes* genome and compared their expression in the transcriptomes of three tissues (Fig. 2; Supplementary Data Set 1). Briefly, the VHA holoenzyme typically present in animals is comprised of 14 subunits organized into a V_1 cytosolic domain (subunits A-H) and a V_0 membrane domain (subunits a, c, c", d, e and S1-like) (Fig. 2A)[34]. All these subunits are necessary for function, and appear coordinately expressed (Fig. 2B). Mining of published RNAseq datasets from three juvenile squid organs[35] revealed relatively high mRNA expression in the light organ for the VHA holoenzyme components, including the B subunit (VHA_B)[15] (Fig. 2B). Such expression argues for an elevated activity

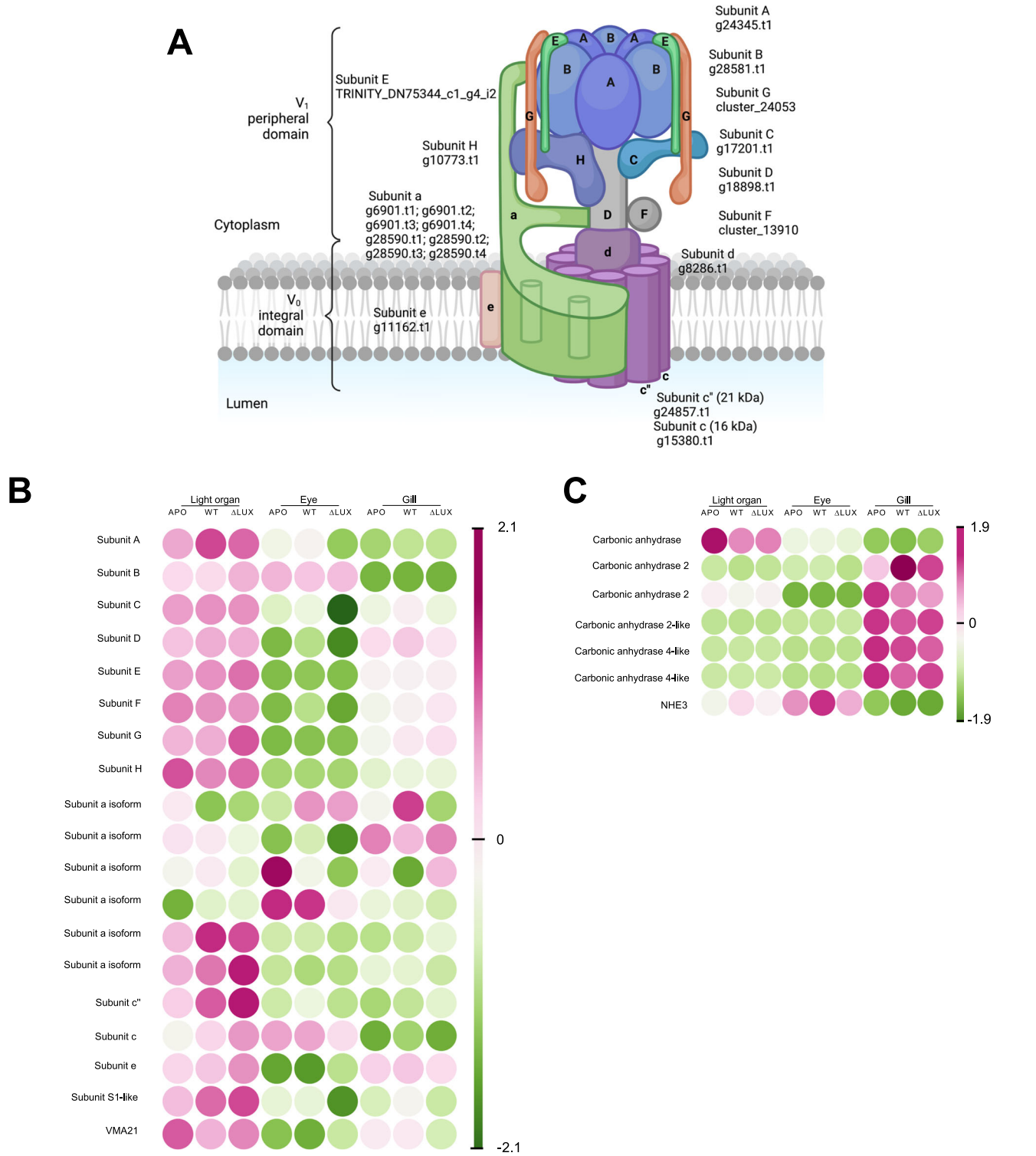

Fig. 2 | Transcriptional expression profiles of juvenile *E. scolopes* genes encoding subunits of the V-type proton ATPase (VHA). A Cartoon of VHA predicted from the genome of *E. scolopes*. **B** Heatmap showing the genes encoding VHA subunits and assembly proteins, as well as their expression profiles across three different organs [light organ (LO), eye and gill] 24 h after hatching (data from ref. 35). In these animals the light organ either remained aposymbiotic or was colonized with either the native bioluminescent strain ES114 (WT), or a dark-mutant derivative of ES114 (ΔLUX). **C** Heatmap depicting the expression of *E. scolopes* carbonic anhydrase (CA) genes and a sodium-proton transporter (NHE3) predicted to be involved in acid-base regulation. Gene counts (rows) were Z-transformed, i.e., scaled to have mean of zero, with a standard deviation of 2.1 (**B**) or 1.9 (**C**); dark magenta indicates highest expression and dark green indicates lowest. Only genes with a >1 TMM expression value in at least one sample are listed. See Supplementary Data Set 1 for the raw dataset including those genes with <1 TMM expression, and for the entire transcriptomic and genomic blast alignments.

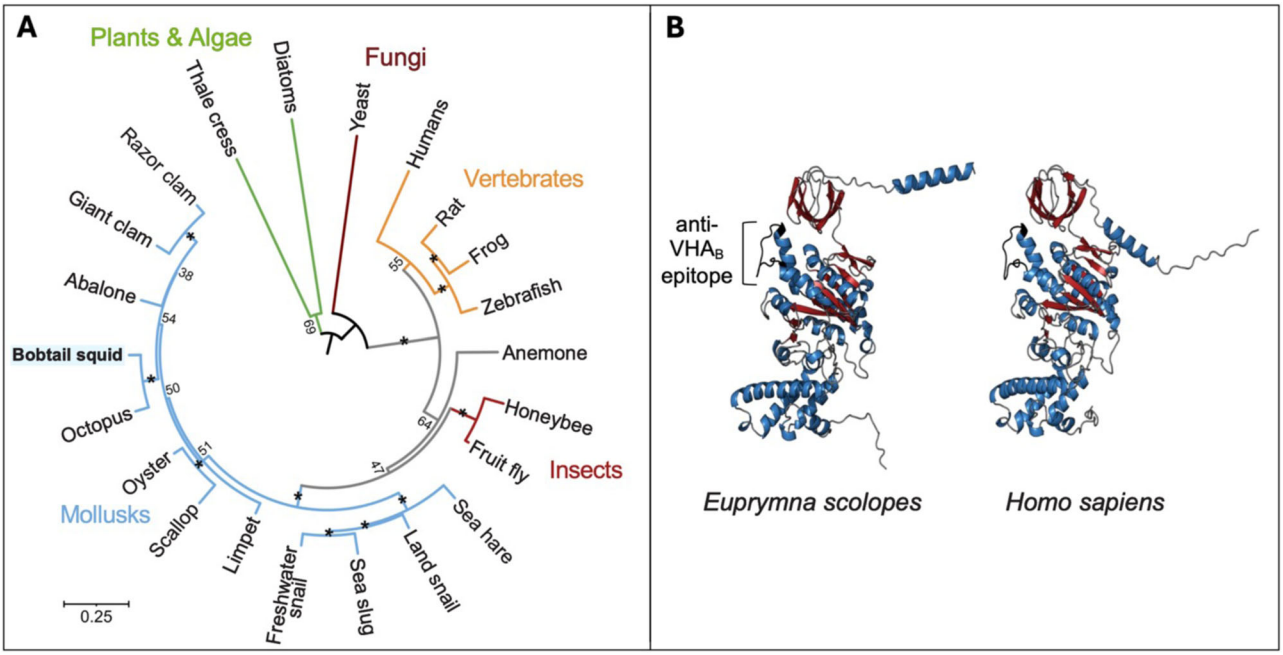

Fig. 3 | Phylogenetic and structural analyses showing a strong conservation of subunit B of VHA (VHA$_B$). **A** Phylogenetic relationships among VHA$_B$ proteins. Numbers at nodes indicate bootstrap values; an asterisk (*) indicates a value above 75%. Scale bar, number of amino acid substitutions per site. **B** AlphaFold-derived models predicting that VHA$_B$ proteins show a high degree of conformational conservation between humans (*Homo sapiens*) and bobtail squid (*Euprymna scolopes*). The position of the epitope used to develop the VHA$_B$ antibody used in this study is indicated by the brackets (see Methods for sequence of this region). Protein coloring denotes secondary structure: red, beta-pleated sheet; blue, alpha helix; black, random coil.

in the light organ, even when compared to gill, a tissue that is typically characterized by high levels of ionic pumping[36].

To determine the evolutionary relationship of the *E. scolopes* VHA$_B$, peptide sequences from subunits across the Eukarya were aligned and a phylogenetic tree was constructed (Fig. 3A). The position of the *E. scolopes* VHA$_B$ reflected evolutionary relationships across organisms, with the squid sequence nesting well within the mollusks. Although subunit amino-acid sequence identities ranged from 75% to 95%, the epitope to which we designed a VHA$_B$ antibody is 100% conserved among animals, with only a single difference [phenylalanine (F) to tyrosine (Y)] in the epitope of yeast, cress and diatom phylotypes (Supplementary Fig. 1).

A comparison of the bobtail squid and human VHA$_B$ subunits revealed an 85% sequence similarity and a strong conservation of structure based on AlphaFold predictions (Fig. 3B). The structures also indicated that the epitope binding site is likely to be easily accessible to antibody interaction. Further, the cytosolic location of VHA$_B$ facilitates antibody binding to the native protein; for these reasons, VHA$_B$ has been a useful target for establishing the cellular and subcellular localization of the VHA holoenzyme using immunocytochemistry (ICC)[37,38]. A western blot of 30 µg of a whole body lysate of hatchling *E. scolopes* confirmed specificity of the antibody, with a single band at the predicted molecular mass (~56 kD) of VHA$_B$ (Supplementary Fig. 2A).

Using this antibody, we performed ICC to determine the tissue locations of the VHA$_B$ protein as a proxy for the VHA holoenzyme. In non-symbiotic tissues of juvenile *E. scolopes*, VHA$_B$ was conspicuous in the apical surfaces of gills (Supplementary Fig. 2B), hemocytes (Supplementary Fig. 2C), and tentacles (Supplementary Fig. 2D). Focusing specifically on the juvenile light organ, confocal ICC showed αVHA$_B$ localizing to the apical area of the epithelial cells comprising the superficial ciliated fields, including strong labeling in the apical perinuclear region (Fig. 4A, B, B'). In addition, tissue sections of these regions revealed labeling of the apical membrane and cilia (Fig. 4C, C', D, D'). Subsequent experiments with the pH-sensitive fluorochrome LysoSensor provided evidence for acidic compartments in intimate association with the nuclei (Fig. 4E) matching the perinuclear localization of VHA$_B$ that was visualized using immune-transmission-electron-microscopy (Fig. 4F) (Supplementary Fig. 2E, E'). While we do not know the identity of these VHA-containing acidic structures, they are likely to be involved in the synthesis and secretion of acidic mucus into the lumen of the light organ. Taken together, these data demonstrate that VHA is abundantly present and active in various subcellular localizations within the apical region of light-organ cells before colonization, and suggest a role for VHA in the initiation of the association.

Our findings of VHA association with symbiotic tissues of *E. scolopes* is similar to previous reports describing this protein's occurrence in several other marine invertebrates. For example, giant clams of the genus *Tridacna*, another mollusk taxon, have VHA in the apical surfaces of the gut epithelium that host their extracellular photosynthetic symbionts (Symbiodiniaceae dinoflagellates)[31]. Corals[33] and anemones[32] use VHA to acidify the symbiosome that houses their intracellular photosymbiotic dinoflagellate algae. Further, VHA also occurs in the apical membranes of branchial epithelia in the deep-sea tubeworms, *Riftia pachytila*[39] and *Osedax* spp[30]., as well as in the epithelial lysosomes of the deep-sea mussel *Bathymodiolus japonicus*[40]. These latter three species thrive in nutrient-poor environments through a symbiotic interaction with chemosynthetic bacteria, and VHA is a critical element in regulating nutritional state[41]. In the symbiotic tissues of these marine mollusks, annelids, and cnidarians, VHA colocalizes with carbonic anhydrase (CA), and the two enzymes work together to concentrate CO_2 in the microbial microenvironment, fueling photosynthesis or chemosynthesis. Interestingly, relative to two other tissues examined[35], the squid light organ expresses a high abundance of mRNA encoding one CA isoform (Fig. 2C; Supplementary Data Set 1) that is closely related to CAs from invertebrates[42–44], as well as lower levels of the CA2 and CA4 proteins that have been extensively studied in both invertebrates[43] and vertebrates[45]. These enzymes could provide VHA with proton substrate at the elevated rate necessary to sustain vigorous acidification of the light-organ surface. VHA has also been reported to be involved in acidifing the apical surfaces of mammalian epithelial tissues that harbor complex microbiomes, e.g., the lung airway[21] and intestine[46,47]; however, to our knowledge, the potential role(s) of this VHA activity in modulating microbial dynamics in mammals has not been explored.

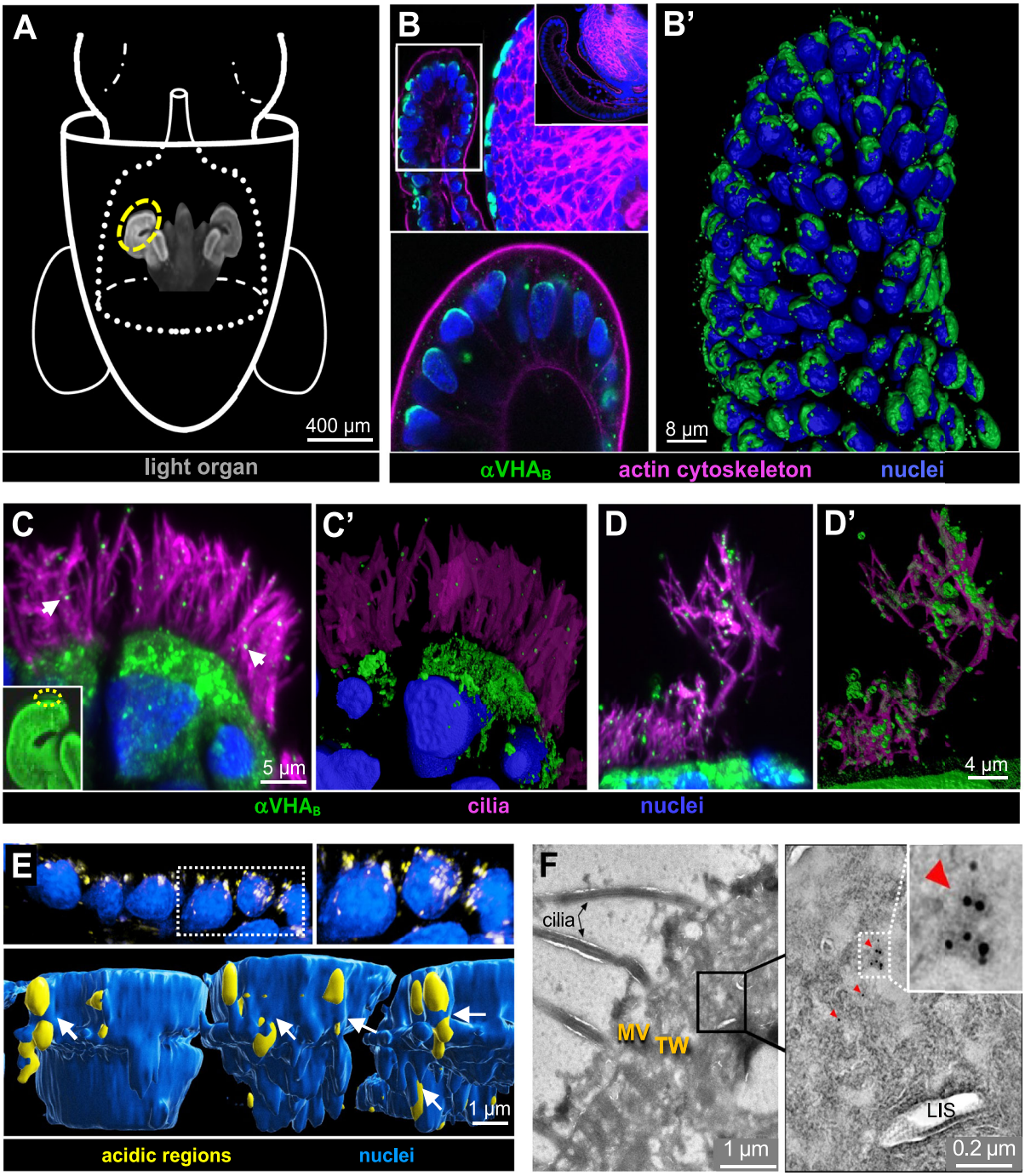

Fig. 4 | Immunocytochemical (ICC) localization of the VHA$_B$ protein within the ciliated fields of the juvenile light organ's superficial epithelium. **A** Illustration indicating the position of the light organ in the mantle cavity, and the appendage tissues (dashed yellow oval indicates one anterior appendage) showing the region of cells displayed in the rest of this figure. **B**, **B'** Confocal microscopy image of areas of VHA$_B$-antibody (αVHA$_B$) labeling. **B** Labeling occurred in the apical surfaces of the epithelium (white box), enlarged below and in (**B'**). Inset: ICC control staining showed undetectable labeling. **B'** Imaris 3D rendering highlighting the close association of the antibody with the epithelial nuclei. **C**, **C'** At higher sensitivity, labeling of host cilia was detected. **C** Confocal image of antibody labeling (white arrows). **C'** Imaris rendering. **D**, **D'** Increased magnification and Imaris rendering. **E** *Upper*, low and high magnification images of LysoSensor-stained acidic regions associated with epithelial nuclei; *lower*, Imaris rendering at even higher magnification, providing evidence that the nuclear regions wrap around (white arrows) the acidic regions. **F** Immuno-electron micrograph of the distal edges of ciliated epithelial cells. Left, an image defining the ciliated region; *right*, enlargement of the area in the black box, including points of VHA$_B$ labeling (red arrows). LIS, lateral intracellular space; MV, microvilli; TW, terminal web.

The localization of VHA in epithelial membranes is typical of non-symbiotic tissues as well. Notably, in a variety of species, VHA is involved in protein sorting in the apical membranes of epithelia, and in the creation of extracellular acidic regions [for reviews see refs. 48,49]. The presence of VHA in ciliated epithelia and its role in the control of ciliary function has also been reported; for example, VHA occurs in the ocular ciliary epithelium, where it has a role in physiological homeostasis[50]. However, to our knowledge, the presence of the VHA protein in the membranes of cilia themselves has not been reported. The extracellular functions of VHA are particularly interesting in the context of the squid-vibrio symbiosis because, as described below, a low pH environment within the mucus shed from the ciliated light organ surface is expected to

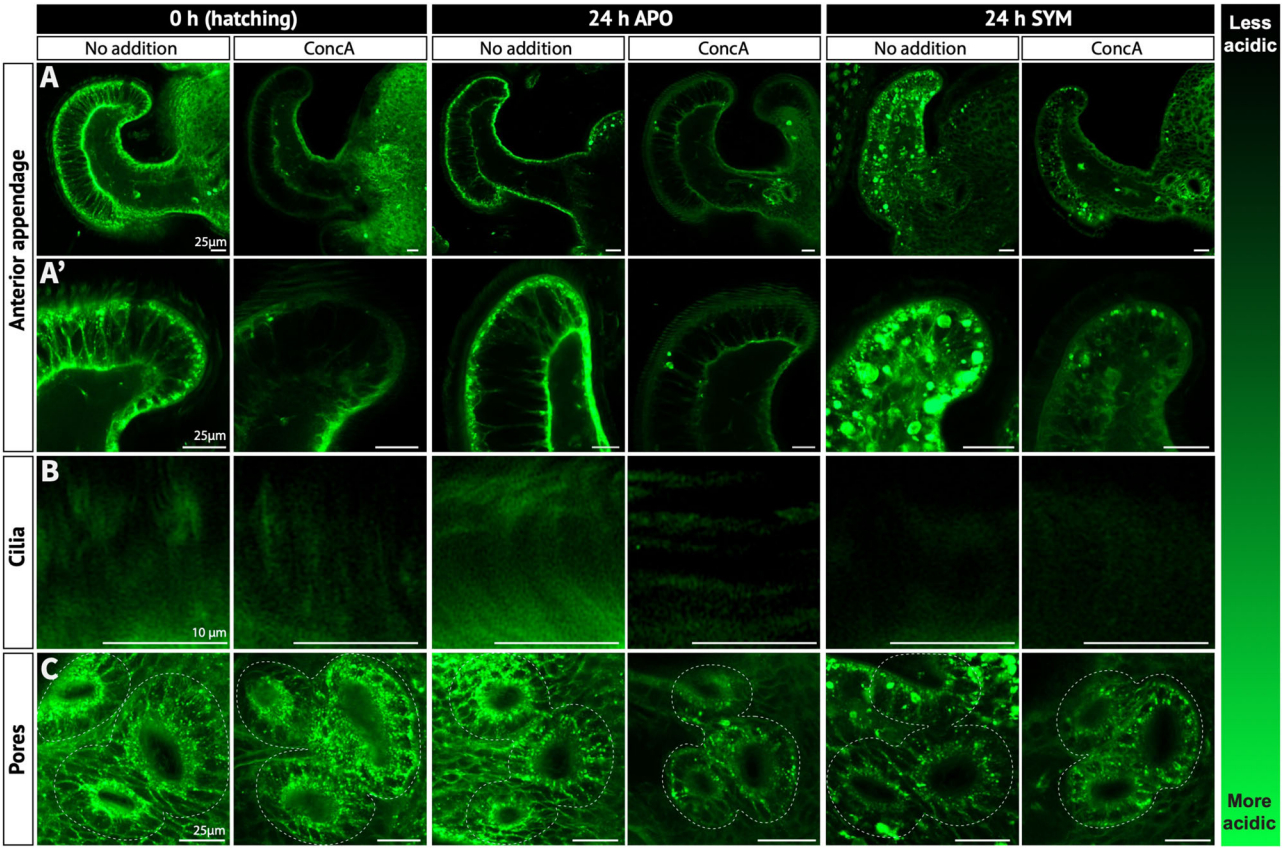

Fig. 5 | Evidence for VHA activity in the living squid light organ at different colonization times, and under different conditions, during the early stages of symbiosis development. The relative acidity of regions of the light organ's superficial ciliated fields in 0-h hatchling, 24-h aposymbiotic (APO) and 24-h symbiotic (SYM) animals was revealed by incubation with LysoSensor (green) in the presence or absence of the VHA inhibitor concanamycin A (ConcA); samples were visualized by confocal microscopy (see Methods for details). **A**, **A'** representative images at low and high magnifications, respectively, of the anterior appendages. The appendages of both hatchling and 24-h APO animals had similar patterns of LysoSensor labeling, with bright regions at the apical and basal surfaces of the cells. After ConcA exposure, both hatchling and APO squid had attenuated signal in these regions. In contrast, the apical and basal surfaces of the SYM animals had similar labeling, with additional labeling both in hemocytes that had entered the blood sinus of the appendage and in epithelial cells that were undergoing symbiosis-induced cell death. The presence of ConcA also diminished the pattern of acidity in SYM animals. **B** Higher magnification images revealed areas of acidity in the region of the cilia. ConcA diminished the degree of staining in both hatchling and APO animals; SYM animals had no labeling in the cilia with or without ConcA. **C** LysoSensor staining around the pores was similar in hatchling animals under both untreated and ConcA-treated conditions but was diminished in ConcA treated 24-h APO animals. Both untreated and ConcA-treated SYM animals showed similar, comparatively low-level staining with LysoSensor. All scale bars, 25 µm; $n = 15$ for each condition (3 clutches, 5 animals/clutch).

enhance biochemical activities that promote the recruitment of its specific symbiont[7].

VHA activity acidifies the superficial ciliated cells of the light organ and is affected by symbiosis onset

To provide functional evidence for the role of VHA in the light organ of *E. scolopes*, the degree of acidity in cells of the superficial ciliated field of the light organ was visualized using the fluorescent dye LysoSensor, a pH indicator, in the absence and presence of a 30-min exposure to the highly specific VHA inhibitor, concanamycin A (ConcA) in live-animal tissues. This plecomacrolide inhibits VHA holoenzyme activity with very high specificity by binding to amino acids in the VHA c-subunit that are conserved from yeast to human[51,52] and has been confirmed to be effective against the VHA of all eukaryotes tested including yeast, algae, plants, and animals[53–56]. In addition, nanomolar concentrations of ConcA have been shown not to inhibit structurally similar enzymes such as F- and P-ATPases.

To evaluate the effect of VHA activity across time and in response to symbiosis, juvenile squid were raised either aposymbiotically (APO), i.e., without exposure to *V. fischeri*, or symbiotically (SYM), i.e., after a 24-h exposure to *V. fischeri*. Because ConcA did not influence *V. fischeri* growth in culture (Supplementary Fig. 3), we were encouraged to use this inhibitor during the colonization process. Juvenile squid that were treated with up to 5 nM ConcA for as long as 24 h (8 times the exposure length used in this experiment) showed no sign of reduced viability or behavioral abnormality, nor a reduction in bioluminescence, the signature activity of the symbiosis, for up to 4 days.

In these experiments, juveniles were incubated with LysoSensor, either with (ConcA in DMSO) or without (DMSO alone) ConcA, immediately prior to imaging. (For details of protocols associated with imaging, see Methods section "Live imaging of the host with a pH-sensitive fluorochrome".) Immediately after hatching (0 h), squid incubated in seawater or seawater containing the solvent control, DMSO, showed punctate regions of high acidity (low pH) along the basement membranes and the apical cytoplasmic regions (Fig. 4A, A' left panels), as well as along the cilia (Fig. 4B, leftpanels) and pore regions (Fig. 4C, left panels) of the organ. In newly hatched squid, this acidity was diminished in most regions when the VHA inhibitor ConcA was added, i.e., the pH was higher, although acidity of the pore region was not as affected. The 24-h APO squid in DMSO alone showed a similar pattern of LysoSensor labeling from newly hatched squid (Fig. 5 A, A', B, C, middle panels). In contrast, 24-h SYM squid in DMSO alone showed a dramatic increase in acidic regions across the anterior appendage, a signature pattern that occurred following symbiont-induced

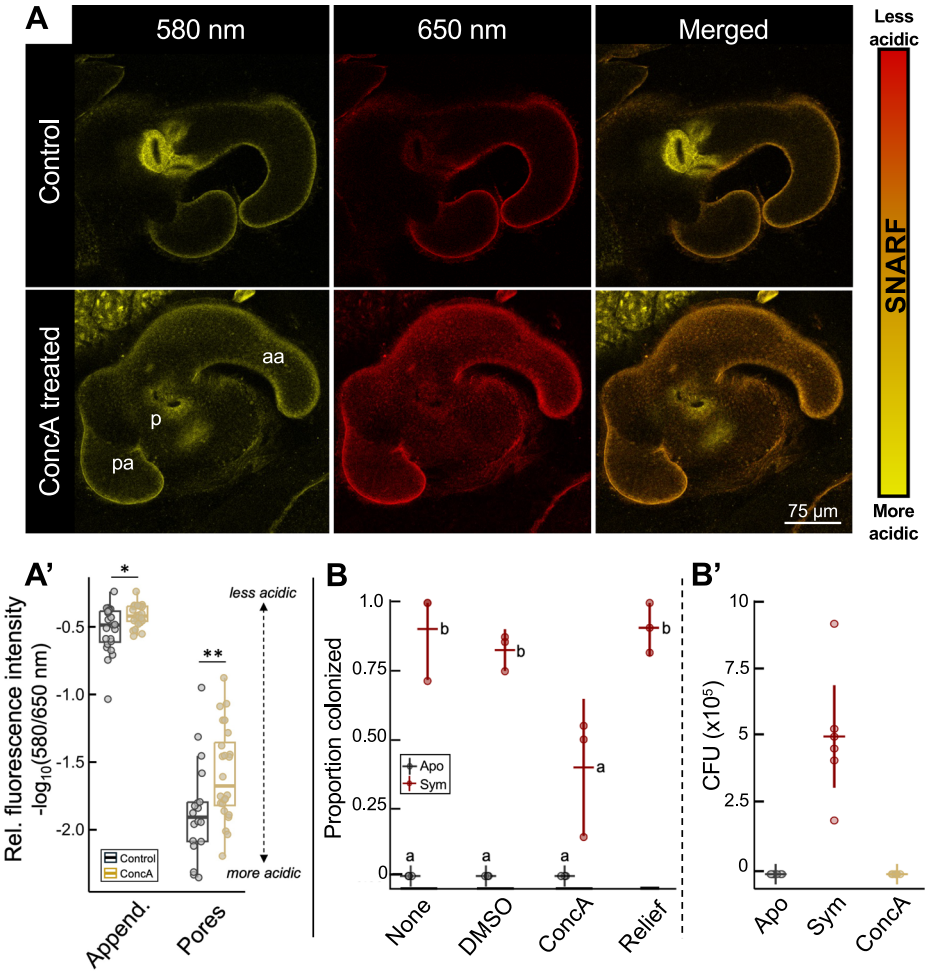

Fig. 6 | The impact on colonization of the mucosal pH gradient present along the hatchling light-organ surface. A, A' Tissue pH is indicated by the ratio of fluorescence emissions of the fluorochrome SNARF at 580 and 650 nm. **A** Fluorescence of SNARF associated with tissue surfaces indicated a sharp pH gradient from the more acidic pore region to the less acidic appendages (upper row), which was reduced when the VHA-inhibitor ConcA was present (lower row); aa, anterior appendage; p, pore; pa, posterior appendage. **A'** Effect of ConcA treatment on the relative fluorescence intensities in two tissue regions, the appendages (Append.) and the pores, of the organ surface. Each point represents a single squid; n = between 21–24 squid; Bonferroni-corrected, independent Mann–Whitney U tests; $^{*}p < 0.05$, $^{**}p < 0.01$. Impact of VHA inhibition on light-organ colonization. **B** Colonization efficiency, as measured by the proportion of squid becoming luminous after 18 h, was reduced when the squid had been inoculated for 3 h in the presence of 1 nM VHA-inhibitor ConcA. Letters (a, b) represent statistically different mean values ($p < 0.05$); each point represents a replicate; n = between 7–15 squid/treatment per replicate. Error bars represent 95% confidence intervals. Juveniles treated for 3 h with ConcA, washed, and then inoculated (Relief) were as efficiently colonized as untreated animals (**B'**). Average number of colony-forming units (CFUs) per light organ after 18 h under different treatments. *V. fischeri* cells were not present in the light organs of the uncolonized (non-luminous) ConcA-treated juveniles from (**B**); $n = 5$ squid/treatment.

morphogenesis in regions of widespread symbiont-induced cell death and hemocyte trafficking (Fig. 5A, A' B, C, right panels); acidification of these areas has been previously reported[57,58].

When VHA activity was inhibited with ConcA, acidic regions labeled by LysoSensor were similarly diminished in the epithelial cells of the anterior appendages across both 24-h APO and SYM, whereas the cilia and the pores showed different patterns of acidification. While APO squid showed acidic cilia attenuated with ConcA treatment, both ConcA treated and untreated SYM squid showed attenuated or undetectable acidity in the cilia, which are still present on the appendages at this timepoint (Supplementary Figs. 4, 5A). Given the ICC detection of VHA protein in the cilia of SYM animals (Supplementary Fig. 5B), the data suggest that symbiosis inactivates VHA in the cilia. The loss of VHA activity in the cilia at 24 h occurs concomitantly with previously reported loss of mucus shedding and *V. fischeri*-cell aggregation by this time in the colonization process[12]. In contrast with the patterns in the cilia, no reproducible difference in LysoSensor signal in the pores was observed between 24-h APO and SYM and labeling in neither region changed reproducibly with ConcA inhibition of VHA. In addition, ICC showed low levels of VHA labeling of the cells immediately surrounding the pores (Fig. 5 APO and SYM, Pores/no Addition; Supplementary Fig. 5B). The low abundance of VHA at the pores and the retention of the acidic signal in the pore regions with ConcA inhibition suggest the presence of another, as yet unknown, acidifying biochemistry in these regions.

These experiments revealed the pattens of VHA-driven acidity in the superficial epithelial cells of the organ using the specific inhibitor ConcA. Other regions, most notably around the pore, retained LysoSensor labeling even in the presence of ConcA inhibition, suggesting either the possibility of other acidifying biochemical mechanisms beyond VHA or that the penetrance or concentration of ConcA is not sufficient to attenuate the LysoSensor labeling completely. These technical caveats aside, the data establish that, once the bacteria have entered the pores, the VHA-mediated acidity in the ciliated fields is no longer a critical factor.

Embryogenesis poises the extracellular light-organ surface to exploit VHA activity, whose inhibition compromises the efficiency of symbiont colonization

As mentioned, a complex array of anatomical, biochemical and biophysical features develops during embryogenesis to prepare the animal for symbiont recruitment (for review, see ref. 7). Previously reported work[10] demonstrated a strong pH gradient across the extracellular, mucus-rich environment of the ciliated fields at 3 h post-hatch, i.e., from the seawater (pH ~ 8) to the light-organ pores (pH ~ 6). This gradient constitutes a 100-fold change in H^+ concentration in the mucus over a distance of ~200 µm, from the appendage tips to the pores (Fig. 1, right). Both the location of VHA in the hatchling light organ (Fig. 4) and the attenuation by ConcA of LysoSensor staining in the apical surfaces of the light-organ superficial epithelia (Fig. 5) suggest that at hatching VHA plays a role in acidifying the mucus surrounding the light-organ appendages. To test this hypothesis, we modified methods developed by Kremer et al.[10] and, sought to determine whether during embryogenesis VHA-dependent acidification in cells along the light-organ's surface helps prepare this tissue for the specific recruitment of *V. fischeri* upon hatching.

At hatching, animals have not yet begun to shed copious amounts of mucus, although a thin patina covers the organ surface (Fig. 6A). Soon thereafter, mucus begins to accumulate extracellularly[12], producing a pH

gradient that develops from the proximal pore region (more acidic) to the distal appendages (less acidic). This gradient can be visualized by staining with SNARF, a membrane-impermeant pH-sensitive fluorescent dye, conjugated to wheat germ agglutinin (WGA), which binds to the mucus (Fig. 6). The ratio in the fluorescence emission levels (580/650 nm) of SNARF changes with the ambient pH, which can be estimated by a calibration curve (Supplementary Fig. 6). Importantly, we found that in the presence of ConcA, the mucus around the light-organ appendages, and especially the pores, was significantly less acidic (Fig. 6A'; Supplementary Data Set 2). The high level of 580 nm emission by extracellular SNARF near the pores in hatchling animals, which is reduced after ConcA treatment (Fig. 6A), is consistent with previous reports[10] that this region is the most acidic, and supports the hypothesis that the pores are the biochemical 'gatekeepers' of the light organ; that is, no other species of bacteria have been found to be alive beyond these entrances to the migration paths[59].

Because VHA is an abundant protein in the ciliated cells that potentiate colonization, we sought to determine whether its activity plays a role in *V. fischeri* colonization. Indeed, animals treated with ConcA were significantly impaired ($X^2_{(6, N=32-56)} = 64.64$; $p << 0.001$); Fig. 6B; Supplementary Data Set 2) in colonization efficiency; specifically, using the presence of detectable bacterial luminescence as a proxy for colonization, an average of only ~30% of ConcA-treated squid were successfully colonized under conditions that led to a ~ 90% colonization of untreated squid ($p < 0.001$; $Z = 4.1$). In contrast, squid treated with the solvent control (DMSO) showed no statistical reduction in colonization efficiency ($p = 1$; $Z = 0.73$). To eliminate the possibility that ConcA-treatment was attenuating luminescence, rather than inhibiting colonization, the light organs of non-luminous, ConcA-treated animals were plated to determine the presence of *V. fischeri* colony-forming units (CFUs). Because no CFUs were detected (Fig. 6B'; Supplementary Data Set 2), and ConcA has no effect on growth or luminescence in culture (Supplementary Fig. 3) we concluded that ConcA had influenced colonization, not symbiont light production. Finally, to determine whether this inhibition of colonization was reversible, ConcA-treated squid were transferred into untreated seawater containing a *V. fischeri* inoculum. After an additional 24 h, these squid (Relief) were observed to be as effectively colonized as controls ($p = 1$; $Z = 0.173$) (Fig. 6B; Supplementary Data Set 2), establishing that ConcA treatment has no apparent lasting impact on the host such as might be expected from a possible effect on neural activity[60]. Taken together, our data align well with recent studies demonstrating that mucus shedding, which occurs within minutes of hatching and is characterized by an acidic signature and abundant low-pH-activated antimicrobials, is essential for efficient colonization, and that VHA plays a role in this acidification and the subsequent recruitment of symbionts[61].

Normal aggregation of *V. fischeri* during recruitment relies on VHA activity

As demonstrated above, the impact of VHA on colonization could take place at any point throughout the process, i.e., at the aggregation stage, during entry through the pores, along the migration path, or in the crypt spaces. Data presented here and in previous studies suggest that VHA plays a key role in the aggregation phase of the symbiont's recruitment process by acidifying the extracellular mucus microenvironment. These data include: the abundance of VHA within cells of the light-organ surface (Fig. 4); the VHA-dependent acidity of the shed mucus where *V. fischeri* cells aggregate (Figs. 5, 6)[10]; and the presence in this mucus of a complex variety of 'antimicrobials' that require low pH for activity[7]. Further, the report that specificity is determined during aggregate formation and that only *V. fischeri* cells survive entry into the migration path through the pores[59] suggest a central role for VHA in the selection of the symbionts. Thus, we sought to determine whether VHA activity is critical for the specific aggregation of *V. fischeri* cells on the light-organ surface (Fig. 7) as well as for successful passage of *V. fischeri* cells into the migration pathway (Supplementary Fig. 7).

We first examined the impact of VHA inhibition on bacterial aggregation on the light-organ surface of various *V. fischeri* strains (Fig. 7A; Supplementary Data Set 3). To allow for prolonged visualization of the aggregation stage using confocal microscopy, we inoculated with two *V. fischeri* motility mutants, as they are competent to aggregate but cannot move into the migration path of the organ. Both mutants of the wild-type strain ES114, Δ*motB* lacking flagellar rotation and Δ*flrA* lacking the flagellum itself[62], showed comparable aggregation size to wild-type ES114 under typical colonization conditions (Fig. 7A; Supplementary Data Set 3). With exposure to ConcA, mean aggregate size of both ES114 and Δ*motB* were significantly reduced (ES114; $p < 0.01$; $U = 299$; $n = 19$, Δ*motB*; $p < 0.01$; $U = 275.5$; $n = 18$), while the aggregate size of Δ*flrA* was lower but not significantly affected ($p = 0.33$; $U = 275.5$; $n = 19$). Another wild-type *V. fischeri* strain, MB13B2, known for quickly forming larger aggregates[63], showed greater variability in aggregate size than ES114 under normal conditions. Though not a statistically significant effect, the addition of ConcA also reduced MB13B2 aggregate size ($p = 0.93$; $U = 272.0$; n = 12). These findings suggest that *V. fischeri* cells benefit from the acidic microenvironment generated by VHA to aggregate efficiently at the surface of the light organ, where in nature it must successfully compete with ~10^6 nonspecific members of the bacterioplankton per milliliter of seawater.

Under natural conditions, planktonic *V. fischeri* cells constitute a very small proportion of the microbial community in the water column [typically < ~0.1%[64];] and, in their absence, other Gram-negative bacteria will aggregate at the light-organ surface, with non-symbiotic *Vibrio* spp. being most effective in this behavior[59,63]. To determine how acidity influences competition, aggregation of *V. fischeri* ES114 was compared to the aggregation of a non-symbiotic Gram-negative bacterium, *Vibrio campbellii* KNH1, in the presence and absence of ConcA (Fig. 7B; Supplementary Data Set 3). This *V. campbellii* strain was chosen as it is a non-symbiotic, natural isolate from the squid host's habitat in Hawaii[13]. The interaction of ConcA treatment and the specific strain was a significant factor in explaining the size of the aggregates ($F_{(1,81)} = 21.61$; $p < 0.001$; $n = 21–23$). In agreement with Fig. 7A *V. fischeri* (ES114) showed reduced aggregate formation when VHA was inhibited ($p < 0.0001$). In the absence of *V. fischeri* in the water, *V. campbellii* could aggregate, but these aggregates were significantly smaller than those made by *V. fischeri* ($p < 0.03$). During VHA inhibition, *V. campbellii* cells formed larger aggregates than with the DMSO control and were not significantly different than the size of control *V. fischeri* aggregates ($p = 0.39$) (Fig. 7B; Supplementary Data Set 3). These data suggest that *V. fischeri* thrives in the acidic natural microenvironment created by the host, while *V. campbellii* does comparatively poorly. However, when VHA-dependent acidification was reduced by ConcA, *V. fischeri* was unable to establish large aggregates while *V. campbellii* was. Similarly, when squid were co-inoculated with both *Vibrio* species, (i.e., 50% ES114: 50% KNH1), *V. fischeri* aggregated as a greater proportion than *V. campbellii* (Fig. 7C; Supplementary Data Set 3). However, ConcA treatment resulted in *V. fischeri* losing its competitive advantage; instead, *V. campbellii* now constituted a greater proportion ($p < 0.01$; $U = 99.5$; $n = 20$) of the aggregate. These observations provide evidence that VHA-dependent acidification enhances *V. fischeri* dominance at the surface of the light organ, where they then outcompete other bacteria for aggregation.

Under normal conditions, no live bacteria other than *V. fischeri* have been observed in the pores and migration path[59] and, thus, we determined whether *V. campbelli* can enter the ducts and remain vital when VHA is inhibited. The use of a fluorescent dye that distinguishes living from metabolically compromised or dead bacteria, revealed that, while *V. fischeri* cells were alive within the ducts, no living *V. campbellii* cells were detected in the migration path beyond the pores regardless of VHA inhibition (Supplementary Fig. 7). These data provide evidence that, while VHA is critical for specificity of microbial symbionts on the light-organ surface, a VHA-independent mechanism(s) plays a role in specificity beyond the pores.

This study adds to previous reports on the function of VHA in the beneficial associations of animals as diverse as giant clams[31], cnidarians[32,33], and annelids[30,39], contributing to an emerging picture that VHA-dependent acidification by host cells may play a ubiquitous role in shaping symbioses between aquatic invertebrates and microbes. Furthermore, VHA exhibits both structural and functional evolutionary conservation among diverse

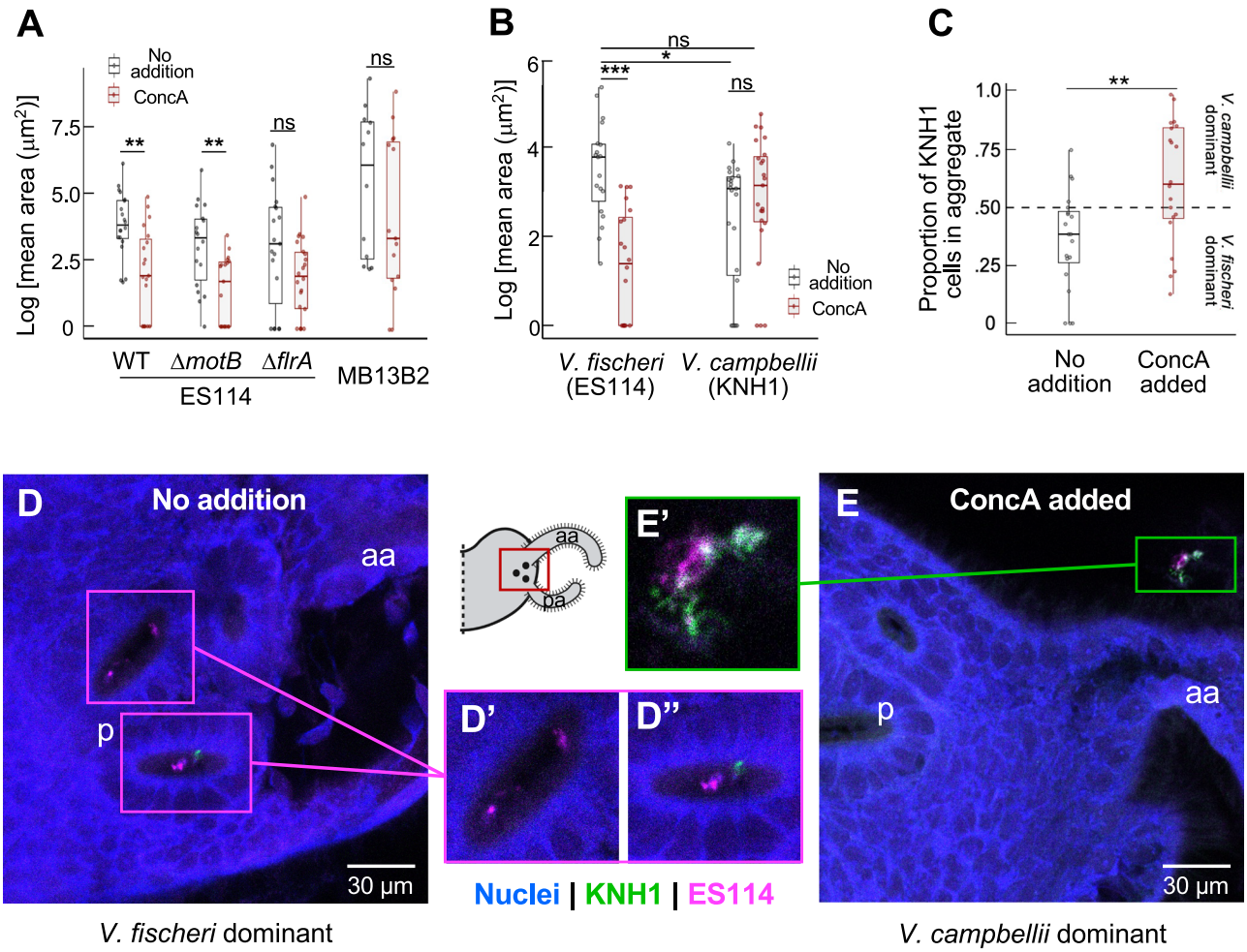

Fig. 7 | The impact of VHA activity on *V. fischeri* aggregate formation at or near the pores on the light-organ surface. Measurements were performed based on confocal images. **A** Two strains of *V. fischeri* showed significantly reduced aggregate size in the presence of the VHA inhibitor ConcA: wild-type (WT) strain ES114 and its Δ*motB* derivative (a nonmotile mutant in the flagellar motor); $n = 18$; $^{**}p < 0.01$. In contrast, while ConcA decreased the average size of aggregates made by either another ES114 derivative, Δ*flrA* (a mutant lacking any flagella; n = 19, p = 0.33), or wild-type MB13B2 (a strain that typically makes very large aggregates; $n = 12$, $p = 0.93$), the differences were not statistically significant (ns). Each point is representative of the average aggregate size for each light organ (including both left and right sides) at 3 h post-hatch. **B** *V. campbellii* strain KNH1, $n = 23$, typically formed a smaller aggregate than *V. fischeri* ES114, $n = 19$, $p = 0.03$; however, while VHA inhibition by ConcA resulted in a significantly reduced aggregate formation by ES114, $n = 20$, $^{***}p < 0.001$, KNH1 showed no such effect, $n = 23$, $p = 0.54$. (**C**) *V. fischeri* ES114 typically dominates over *V. campbellii* KNH1 in co-aggregation assays, $n = 20$; however, in the presence of ConcA, *V. campbelli* became dominant, $n = 20$, $^{**}p < 0.01$, suggesting that the advantage shown by *V. fischeri* cells was dependent on normal VHA activity of the host. Each point represents the proportion of KNH1 cells relative to the total number of bacteria in the aggregate at 3 h post-hatch. (**D**) In a typical animal used in (**C**), at one pore (p), *V. fischeri* was the only aggregating bacterium (**D'**), while at another, *V. campbellii* was also present (**D"**). **E, E'** In contrast, with the addition of ConcA, *V. campbellii* became numerically dominant over *V. fischeri* in the majority of aggregates. aa, anterior appendage; pa, posterior appendage.

taxa of eukaryotes, including activities as foundational as food digestion and innate immune function[20]. Thus, VHA is poised to also widely mediate selection and maintenance of microbial symbionts by their hosts and, perhaps, may have undiscovered biomedical implications, a hypothesis that deserves further investigation.

The results presented here support a critical role for VHA in shaping the initial colonization of the host by its microbial partner. The data show that, in the squid-vibrio association, VHA-driven acidification of the mucus covering the nascent light organ is a defining feature in the complex series of events unfolding within the first 3 h after initial contact between the host and symbiont cells. Together with other factors[7], VHA acidification enables this environmentally acquired partnership to ensure colonization by the proper symbiont at each host generation, with high specificity and against the background of a diverse ambient bacterioplankton. Thus, the squid-vibrio system provides an invaluable opportunity to discover and analyze the factors that allow a host to select its correct symbionts. Because host-symbiont cell-cell interactions are highly conserved, it is likely that many of the mechanisms underlying selectivity in the squid-vibrio system will apply to the recruitment of bacteria in other horizontally transmitted associations, such as those in the mammalian gut.

Methods

Host collection, husbandry and colonization with the symbiont

Adult *E. scolopes* were collected from the sandy shallow-water flats of the SE shore of Oahu, HI, and maintained in artificial seawater [Instant Ocean® (IO); Spectrum Brands, VA] in water tables at the California Institute of Technology, Pasadena, CA. Animals were ethically treated under the Institute's IACUC-reviewed protocol IA22-1842. Once egg clutches were laid, the eggs were placed in a separate water table under a 12:12-h day-night light cycle. Symbiotic juvenile squid (SYM) were produced by exposing newly hatched juveniles to ~1×10^4 CFUs of *V. fischeri* strain ES114 added per mL of either natural seawater obtained from the pier pump of Scripps Institution of Oceanography (SIO seawater), or unfiltered IO, for 18 h; aposymbiotic juveniles (APO) were kept in (uninoculated) SIO seawater or

unfiltered IO, both of which contained undetectable levels of *V. fischeri*. Preparation of the *V. fischeri* inoculum was performed as previously described[65]; no differences in colonization results were detected when using either of these seawater sources. "Hatchling" squid refers to newly hatched juvenile animals that were used for the "0 h" timepoint. Within 10 min of hatching, they were fixed without exposure to *V. fischeri*. Colonization of SYM animals was confirmed by determining the bioluminescence of juveniles using a TD-20/20 luminometer (Turner Designs, Sunnyvale, CA), and the numbers of symbionts colonizing the organs were estimated by the number of *V. fischeri* CFUs obtained from dilutions of homogenized squid. For experiments lasting longer than 24 h, 100% water changes were performed every day. All experiments used 7–10 juveniles, and each experiment was replicated three times with different clutches to minimize the impact of any genetic variability between animals.

Bioinformatics

To gather homologous sequence information for the VHA B-subunit (VHA_B) across the tree of life, the 56 kDa isoform of the *E. scolopes* VHA_B was obtained from the genome sequence[66] and BLASTed[67] against the NCBI database (as of September 25th, 2023). Sequences were aligned using MAFFT alignment software, v7.520[68] and the phylogenetic relationships were assessed using IQ-Tree, v2[69]. Phylogenetic trees were produced using model (LG + I + G4), and branch support was assessed using one million bootstraps. iTOL interactive tree of life [v6.8.1[70];] was used to visualize the resultant trees. AlphaFold[71] was applied to generate structural predictions for the bobtail squid and human VHA_B proteins.

Confocal immunocytochemistry (ICC)

Unless otherwise stated, all chemicals for confocal ICC of whole light organs were purchased from Sigma-Aldrich (St. Louis, MO). The ICC experiments were performed as previously described[72,73]. Briefly, juvenile squid anesthetized in 2% ethanol in SIO seawater and were fixed overnight at 4 °C with gentle agitation in 4% paraformaldehyde (PFA) in marine phosphate-buffered saline (mPBS: 50 mM sodium phosphate buffer, 450 mM NaCl, pH 7.4). To remove excess fixative, squid were rinsed three times with mPBS and stored in mPBS at 4 °C prior to ICC. All subsequent ICC steps were completed at 4 °C. Whole squid or dissected light organs were placed directly into the permeabilizing solution, mPBS-T (1% Triton X-100 in mPBS). For whole-body ICC, an incision was made along the ventral side of the mantle prior to permeabilization to increase antibody accessibility. Permeabilized tissue was placed in blocking buffer-1 (0.5% bovine serum albumin and 1% normal goat serum, in mPBS-T) with gentle agitation overnight. Following blocking, the sample was incubated for 4 d in blocking buffer-1 with either primary antibody or with the appropriate IgG control. VHA_B was localized using a custom-made purified rabbit polyclonal antibody designed against an epitope (AREEVPGRRGFPGY) in the B-subunit (Supplementary Fig. 1). The resulting antibody (αVHA_B; 0.48 mg mL^{-1}), conjugated to ovalbumin (GenScript, Piscataway, NJ), was used at a 1:500 dilution in blocking buffer-1 (0.96 μg mL^{-1}). Rabbit IgG at the same dilution as αVHA_B was used as a negative control.

The nuclear envelope was immunolabeled using a commercial α-nucleoporin antibody (Cat # 902907; BioLegend, San Diego, CA; 1 mg mL^{-1}) and diluted 1:100 in blocking buffer-1; mouse IgG was the control (10 μg mL^{-1} final concentration). The tissues were rinsed three times with mPBS-T and blocked again overnight. The following day, secondary antibody labeled with either goat anti-rabbit FITC or TRITC (Jackson ImmunoResearch, West Grove, PA; 1.5 mg mL^{-1}) was added at a 1:25 dilution in blocking buffer-1 (60 μg mL^{-1} final concentration), and incubated overnight. After secondary-antibody treatment, the sample was rinsed three times with mPBS-T. TO-PRO-3 DNA stain (1:1000; 1 mM) and phalloidin-405 actin stain (1:40; 66 μM), both purchased from Thermo Fischer Scientific, Irwindale, CA, and diluted in blocking buffer-1, were then added to label nuclei (1 μM final concentration) and F-actin (1.65 μM final concentration), respectively. After a two-day incubation, samples were rinsed three times with mPBS-T, then placed in mPBS and mounted in Vectashield (Vector Laboratories, Newark, CA).

For confocal microscopy of light-organ tissue, PFA-fixed samples were dehydrated, embedded in paraffin wax, and sectioned following previously described protocols[74]. Briefly, tissues were deparaffinized, rehydrated, permeabilized with mPBS-T, and incubated in blocking buffer-2 (0.5% bovine serum albumin, 1% normal goat serum, and 0.5% keyhole-limpet hemocyanin in mPBS-T) for 1 h at room temperature. Sections were incubated overnight at 4 °C, with (i) 0.03 μg of goat-polyclonal anti-VHA_B primary antibody per mL of blocking buffer-2, (ii) antibody with 20-fold excess peptide on a molar basis ("pre-absorption control") in blocking buffer-2, or (iii) blocking buffer-2 alone. Alpha-tubulin was labeled with 0.14 μg mouse-monoclonal antibody per mL (Cat. #12G10, Developmental Studies Hybridoma Bank, Iowa City, IA). Sections were washed with three rinses of mPBS-T (5 min each) before incubation for 1 h with two secondary antibodies (goat anti-rabbit–Alexa Fluor588, and goat anti-mouse–Alexa Fluor568; Invitrogen, Carlsbad, CA) at a final concentration of 4 μg mL^{-1} each in blocking buffer-2 at room temperature. This treatment was followed by an incubation with TO-PRO-3 DNA stain (1 μM final concentration) for 5 min. Sections were then washed three times with mPBS-T (5 min each) to remove unbound secondary antibodies.

Specific confocal microscope and imaging acquisition parameters are listed in Supplementary Table 1. Briefly, light-organ tissue sections were imaged using a Zeiss LSM 800 inverted confocal microscope, and whole-mount light-organ tissue samples were imaged on a Zeiss LSM 900 upright confocal microscope. To control for differences in fluorescence across experiments and microscopes, for each set of samples the laser intensities were lowered to produce minimal fluorescence from control tissues incubated with rabbit IgG. Alexa Fluor 488 and Alexa Fluor 568, and TO-PRO-3 were used to visualize antibodies and DNA, respectively. To facilitate visualization by color-blind readers, αVHA_B, α-tubulin, and TO-PRO-3 signals are presented using the false colors: green, violet, and blue, respectively. Three-dimensional reconstructions of 3.5-μm thick Z-stacks were generated using Imaris 9.0 (Bitplane, Zurich, Switzerland).

Immuno-electron microscopy

Juvenile animals were anesthetized in 2% ethanol in filtered SIO seawater. Squid light organs were then dissected from the body cavity and fixed with 4% PFA in mPBS for 1 h. Samples were infiltrated with 2.1 M sucrose in mPBS overnight at 4 °C with continuous agitation. Samples were then affixed individually to aluminum sectioning stubs, dried of excess liquid by wicking, and frozen in liquid nitrogen. Cryosections (100 nm thick) were cut at −110 °C with a EM UC6/FC6 cryo-ultramicrotome (Leica Microsystems) using a cryo-diamond knife (Diatome, Ltd). Sections were picked up using a wire loop with a drop of 2.3 M sucrose in PBS and transferred to Formvar-coated, carbon-coated, glow-discharged copper-rhodium 100-mesh grids (Electron Microscopy Sciences) and placed in PBS. Grids were incubated with 10% calf serum in PBS to block nonspecific antibody-binding sites, then incubated 2 h with the primary antibody, αVHA_B, diluted in PBS. Grids were rinsed four times for 10 min with PBS, then labeled for 2 h with gold-conjugated secondary antibody (Ted Pella, Inc), also diluted in PBS. Grids were rinsed four times with PBS, then three times with deionized water (dH_2O), then simultaneously negative-stained and embedded with 1% uranyl acetate and 1% methylcellulose in deionized H_2O. Grids were air-dried in wire loops prior to imaging.

Electron tomography

Grids were placed in a Model 2040 dual-axis tomography holder (E.A. Fischione Instruments, Export, PA) and imaged with a Tecnai T12-G2 transmission electron microscope (120 KeV, Thermo Fisher Scientific) equipped with a XP1000 2k x 2k CCD camera (Gatan, Inc., Pleasanton CA). Tomographic tilt-series and large-area montaged overviews were acquired automatically using the SerialEM software package[75]. For tomography, samples were tilted ±62° and images collected at 1° intervals. The grid was

then rotated 90° and a similar series taken about the orthogonal axis. Tomographic data were calculated, analyzed, and modeled using the IMOD software package[75–77] on iMac Pro and Mac Studio M1 computers (Apple, Inc., Cupertino, CA).

Western blot analyses

Samples were prepared by homogenizing five individual hatchling squid in 100 µl of PBS buffer containing protease inhibitor cocktail (Halt 100X Protease Inhibitor Single-Use Cocktail, Thermo Fisher Scientific) as per manufacturer's recommendations. All steps in sample lysate isolation were performed at 4 °C. Homogenized samples were then spun down at 850 × *g* for 10 min to remove ink contamination. The supernatant was collected and centrifuged again at 21,000 × *g* for 15 min to clear particulate material. The resulting supernatant contained the final whole-body soluble protein lysate.

Protein samples (30 µg each) were separated on a 12.5% polyacrylamide gel and transferred at 4 °C to PVDF immunoblotting membrane (Bio-Rad, Hercules, CA). The companion gel was stained with Coomassie blue and imaged to visualize total protein content. Blots were incubated overnight at 4°C with gentle agitation in western blocking buffer, which contained 0.5% BSA and 1% normal goat serum (Thermo Fisher Scientific) in TBS [10-fold diluted Tris-buffered saline (Thermo Fisher Scientific)]. The blots were then probed at 4 °C overnight in either primary antibody (αVHA_B, 1:2500 dilution) or purified IgG, diluted in western blocking buffer (0.19 µg mL^{-1} final concentration. The following morning, the blots were washed three times in TBS containing 0.1% Tween-20 (TBS-T) and incubated for 1 h at room temperature with a 1:10,000 dilution of IRDye 800CW donkey anti-rabbit secondary antibody in buffer per the manufacturer's instructions (Li-Cor Bioscience, Lincoln, NE; 1 mg mL^{-1} final concentration). After washing three times with 0.1% TBS-T, the blots were then imaged using a Li-Cor Odyssey CLx imaging system (Li-Cor Bioscience).

Live imaging of the host with a pH-sensitive fluorochrome

Regions of low pH in light-organ tissues were imaged using LysoSensor Green (DND-189, 1 mM stock; excitation/emission = 443/505 nm; Thermo Fischer Scientific), which fluoresces more intensely in acidic environments. Squid were collected between 11 am–1 pm and either colonized at 2 pm with 5,000 CFUs of strain ES114 per ml of SIO seawater or kept aposymbiotic in uninoculated SIO seawater. At 18 h, the squid were transferred into vials with fresh SIO seawater. Colonization is stochastic among healthy hatchlings; as such, after 24 h, the 10 most luminous SYM animals were selected for analysis, and APO were confirmed as uncolonized. At 1:30 pm (~24 h after hatching), squid were split into treatment groups (APO + 0.001% DMSO, APO + 5 nM ConcA, SYM + 0.001% DMSO, SYM + 5 nM ConcA, $n = 5$ squid each) and added to the appropriate vials with minimal carryover of seawater. Squid were incubated for 30 min in 3 mL of treated or untreated SIO seawater. After 30 min, squid were rinsed three times through vials containing 3 mL of SIO seawater and moved into vials with 3 mL SIO seawater with LysoSensor DND-189 (1:2500 dilution), again with minimal seawater carryover during the transfer. After a 30-min incubation, squid were rinsed again as described above and added to vials with 3 mL of 2% EtOH in SIO seawater for 5 min to anesthetize the squid. Squid were dissected to expose the light organ and mounted with a glass coverslip for imaging immediately after dissection. This procedure was repeated three times on independent clutches to control for genetic variation[78].

Imaging parameters were set to eliminate autofluorescence using squid with no LysoSensor stain added. All squid were imaged with identical parameters for visualizing a LysoSensor signal using a Zeiss LSM 900 upright confocal microscope. Specific microscopy and imaging acquisition parameters are listed in (Supplementary Table 1). Images were processed in Fiji-ImageJ[78] with identical contrast adjustments across all acquisitions. For label-intensity analysis of cilia, images were randomized, presented in gray scale, and scored by three individuals with no knowledge of sample IDs on a scale of: 1-dim, 2-intermediate, 3-bright. All scores were in majority agreement and are summarized in Supplementary Fig. 4.

Measurements of the pH gradient on the organ surface

The gradient of mucus pH was measured as previously described[10,79]. Briefly, wheat germ agglutinin (WGA), which binds to the surface mucus of the host[12], was coupled to the pH-sensitive probe SNARF (both from Thermo Fisher Scientific) in a buffer containing 29 µl of 20 mM 5-(and 6-)-carboxy SNARF^{TM}-1, 100 µl of a 10 mg mL^{-1} solution of WGA, and 371 µl of 50 mM MOPS [3-(*N*-morpholino) propanesulfonic acid] buffer at pH 6.5. This solution was incubated for 15 min at room temperature before the addition of 1.6 µl of a 70 mg mL^{-1} solution of EDAC [1-ethyl-3-(3-dimethylaminopropyl)carbodiimide, hydrochloride] (Thermo Fisher Scientific). The resulting mixture was incubated at room temperature for 30 min and moved to 4 °C overnight. Then, 55 µL of 1 M glycine were added for 30 min at room temperature to quench the reaction and the mixture was filtered through a 4-ml capacity 10 kDa centrifugal filter unit (Amicon, Miami, FL). To estimate the pH gradient across the ciliated surface of the light organs, hatchling animals were incubated for 30 min in a 1:200 dilution of filtered WGA-SNARF solution, and then rinsed in SIO seawater, and anesthetized in 2% ethanol in SIO seawater prior to imaging. Squid were imaged live on a Zeiss LSM 900 upright confocal microscope. Specific confocal microscopy and imaging acquisition parameters used in this study are listed in Supplementary Table 1. The mean fluorescence intensity of 10 µm by 10 µm areas around the pores and on the appendages was measured to calculate the 580/650 ratio of fluorochrome emission. A standard curve relating this ratio to pH was calibrated against solutions of SNARF in citrate-phosphate buffer between pH 3.6 to 7.6 (Supplementary Fig. 6) that were viewed by confocal microscopy, applying the same settings used for imaging animal tissue.

The influence of VHA on *V. fischeri* growth. To determine whether the symbionts were influenced by treatment with the VHA-specific inhibitor ConcA, *V. fischeri* cells were cultured in 12-well microtiter plates containing ConcA (dissolved in DMSO), diluted to a concentration of 2.5 nM, 5 nM, or 10 nM in LBS medium[80]. The plates were shaken continuously at 28 °C, and the OD_{600} of the cultures was monitored over 24 h using a Spectra Max iD5 plate reader (Molecular Devices, San Jose, CA). A solvent control containing only DMSO was also included at a volume equivalent to that of the highest ConcA concentration (i.e., 1 µl of DMSO per 25 mL LBS media).

The influence of VHA on host light-organ colonization by *V. fischeri*

To determine whether VHA activity influences the efficiency of host colonization, we determined the effect on colonization of adding ConcA to the animal's ambient seawater. Initial studies with newly hatched juvenile squid incubated with the inhibitor determined that the squid behaved normally at a ConcA concentration of 5 nM or below, consistent with other findings of inhibitor efficacy[53]. Squid were pre-incubated in SIO seawater containing ConcA at 1, 2.5 or 5 nM for 30 min prior to the addition of 10^4 CFUs of *V. fischeri* per mL of IO. After 3 h, the squid were rinsed 3 times in IO and left overnight. Each animal's luminescence was recorded at 18 h as an indication of a successful colonization, which was confirmed by plating CFUs from homogenized squid. Following inhibitor treatment, ConcA was removed by rinsing, and non-luminescent (i.e., uncolonized) animals were moved to fresh IO, either with or without a *V. fischeri* inoculum, and incubated for an additional 18 h to determine whether the effects of treatment with ConcA were reversible (i.e., the animals became colonized/luminescent).

The influence of VHA on symbiont aggregate formation

To study the impact of VHA activity on the aggregation of symbionts, juvenile squid were exposed to fluorescently labeled bacteria in either single or co-incubations. Depending on the experiment, single-colonization squid were exposed to between 10^3–10^5 CFU of GFP-labeled *V. fischeri* (i.e., wild-type, Δ*motB* or Δ*flrA* strains of ES114, or strain MB13B2) or *V. campbellii* (strain KNH1) per mL of SIO seawater (Supplementary Table 2). Co-incubation assays were performed by exposure to equal concentrations of *V. fischeri* (RFP-labeled ES114) and *V. campbellii*, (GFP-labeled KNH1). Juvenile squid were simultaneously incubated with bacteria, and with or

without 5 nM ConcA. After 3 h of incubation, the animals were anaesthetized with 2% ethanol in SIO seawater for 2–3 min and fixed using the ICC protocol described above. The mantle and funnel were dissected away, and the light-organ nuclei were labeled for at least 2 h with TOTO-3 (Thermo Fisher Scientific) diluted 1:6000 into 1% mPBS-T (1 mM final concentration). Subsequently, samples were washed two times for 10 min each with mPBS-T and mPBS at 4 °C.

The determination of aggregate size was carried out by methods used for previous studies of symbiont recruitment[63]. Bacterial aggregates were imaged using a Zeiss LSM 900 upright confocal microscope. Specific confocal microscope and imaging acquisition parameters are listed in (Supplementary Table 1). Z-stacks were acquired, and maximum projections were generated onto one plane. Bacterial aggregate size was compared among strains using the particle analysis tool of the Fiji-ImageJ imaging software. The area (in μm^2) of green / red (i.e., GFP/RFP) fluorescence was calculated using 2 μm^2 as the minimum threshold for bacterial size.

Determination of whether *V. campbellii* travels past the pores with VHA inhibition

We investigated whether aggregate formation of *V. campbellii* under VHA-inhibited conditions allowed living cells to pass through the pores and into the ducts. Hatchlings were exposed to 5,000 CFU of GFP-labeled *V. fischeri* (ES114) or *V. campbellii* (KNH1) per ml of SIO seawater, with and without the addition of ConcA (5 nM), and simultaneously stained with Live-or-Dye NucFix™ Red (1:2500 dilution, Biotinium, Fremont, CA) to label compromised bacterial cells. After a 6-h incubation, squid were anesthetized and fixed as described above. Light organs were dissected from the juveniles, and the nuclei were stained with DAPI (1:1000) in 1% mPBS-T for two days at 4 °C with gentle agitation. Prior to confocal microscopy, samples were rinsed with 1% mPBS-T three times for 5 min to remove excess dye. Samples were imaged using a Zeiss LSM 900 upright confocal microscope. Specific confocal microscope and imaging acquisition parameters are listed in (Supplementary Table 1). Images were processed using Fiji-ImageJ and analyzed for the presence of live KNH1 cells in the light-organ ducts and antechambers.

Statistical analysis, reproducibility and graphing

Each experiment was replicated with juveniles obtained from at least three independent egg clutches from different females. Each light organ was treated as an independent biological replicate. All graphs and statistics were produced using R Statistical Software (v4.0.2; R Core Team 2020; https://www.R-project.org/) and RStudio (v1.3.959; RStudio Team 2020; http://www.rstudio.com/). Data were imported using the readxl package (v1.3.1; https://cran.r-project.org/web/packages/devtools/index.html) and were cleaned using the dplyr package (v1.0.8; https://dplyr.tidyverse.org/authors.html). Data normality and homoscedasticity were assessed using Shapiro-Wilks tests (car package; v3.1.2; https://www.john-fox.ca/Companion/index.html) and Levene's tests (base R), respectively. Mucus pH (WGA-SNARF) for the two light-organ locations (appendages and pores) was analyzed independently using the non-parametric Mann-Whitney U test. Bonferroni test was used to correct for multiple comparisons. Single colonization by *V. fischeri* cells, and co-incubation aggregate data were analyzed similarly, with the effect of ConcA on each strain being independently analyzed, and then corrected for multiple comparisons (base R). Single-incubation data for *V. campbellii* KNH1 were compared to those for *V. fischeri* ES114 by modeling the interaction of treatment and strain using a linear model. A likelihood ratio test (ANOVA) and Tukey's pairwise comparison (car package) were used to obtain p-values. The role of VHA activity on arm length was calculated in a similar manner. To statistically assess the effect of ConcA on colonization rates, squid with luminescence readings between 10–1000 relative light units were considered colonized. The luminescence-colonization data were fitted to a generalized linear mixed-effect model (bglmer) using the blme package [v1.0.5[81];]. Treatment combination (inhibitor X colonization status) was set as a fixed effect and replicate as a random variable. The family was set to "binomial" and a "fixed prior" was added to account for complete separation in the data. Post-hoc analysis of the model was performed using the multcomp package [v1.4.17[82];] and by applying Tukey all-pair comparisons. The multcomp package and the multcompview package (v0.1.8; https://cran.r-project.org/web/packages/multcompView/index.html) were used to provide letters representing statistically significant groups of values for which $p < 0.05$. Graphs were produced using the ggplot2 library (v3.3.6; https://ggplot2-book.org/), ggpubr (v0.4.0; https://github.com/kassambara/ggpubr/releases), ggtext (v0.1.1; https://wilkelab.org/ggtext/), and the extrafont library (v0.18; https://cran.r-project.org/web/packages/extrafont/index.html).

Reporting summary

Further information on research design is available in the Nature Portfolio Reporting Summary linked to this article.

Data availability

Transcriptomic data was retrieved from Moriano-Gutierrez et al. [35], which have been previously deposited in the GenBank database, the National Center for Biotechnology Information Sequence Read Archive (accession number PRJNA473394). Genomic data can be found at https://github.com/TheaFrances/E.scolopes-V2.2-BRAKER2-gene-annotation[83].

Material availability

All data needed to evaluate the conclusions in the paper are present in the paper and/or the supplementary materials, including 3 primary-data excel files: Supplementary Data Set 1, Supplementary Data Set 2 (Fig. 6 numerical source data) and Supplementary Data Set 3 (Fig. 7 numerical source data).

Received: 1 August 2024; Accepted: 2 December 2024;
Published online: 18 December 2024

References

1. Bright, M. & Bulgheresi, S. A complex journey: transmission of microbial symbionts. *Nat. Rev. Microbiol* **8**, 218–230 (2010).
2. Bry, L., Falk, P. G., Midtvedt, T. & Gordon, J. I. A model of host-microbial interactions in an open mammalian ecosystem. *Science* **273**, 1380–1383 (1996).
3. McFall-Ngai, M. Divining the essence of symbiosis: insights from the squid-vibrio model. *PLoS Biol.* **12**, e1001783 (2014).
4. Guilhot, R., Xuereb, A., Lagmairi, A., Olazcuaga, L. & Fellous, S. Microbiota acquisition and transmission in *Drosophila* flies. *iScience* **26**, 107656 (2023).
5. Powell, J. E., Martinson, V. G., Urban-Mead, K. & Moran, N. A. Routes of acquisition of the gut microbiota of the honey bee *Apis mellifera*. *Appl Environ. Microbiol* **80**, 7378–7387 (2014).
6. Videvall, E. Microbiome maturation during a unique developmental window. *Mol. Ecol.* **29**, 1941–1943 (2020).
7. Nyholm, S. V. & McFall-Ngai, M. J. A lasting symbiosis: how the Hawaiian bobtail squid finds and keeps its bioluminescent bacterial partner. *Nat. Rev. Microbiol* **19**, 666–679 (2021).
8. Jones, B. W. & Nishiguchi, M. K. Counterillumination in the Hawaiian bobtail squid, *Euprymna scolopes* Berry (Mollusca: Cephalopoda). *Mar. Biol.* **144**, 1151–1155 (2004).
9. Visick, K. L., Stabb, E. V. & Ruby, E. G. A lasting symbiosis: how *Vibrio fischeri* finds a squid partner and persists within its natural host. *Nat. Rev. Microbiol* **19**, 654–665 (2021).
10. Kremer, N. et al. Initial symbiont contact orchestrates host-organ-wide transcriptional changes that prime tissue colonization. *Cell Host Microbe* **14**, 183–194 (2013).
11. Malik, E., Dennison, S. R., Harris, F. & Phoenix, D. A. pH dependent antimicrobial peptides and proteins, their mechanisms of action and potential as therapeutic agents. *Pharmaceuticals (Basel)* **9**, 67 (2016).
12. Nyholm, S. V., Deplancke, B., Gaskins, H. R., Apicella, M. A. & McFall-Ngai, M. J. Roles of *Vibrio fischeri* and nonsymbiotic bacteria in the

dynamics of mucus secretion during symbiont colonization of the *Euprymna scolopes* light organ. *Appl. Environ. Microbiol.* **68**, 5113–5122 (2002).
13. Nyholm, S. V., Stabb, E. V., Ruby, E. G. & McFall-Ngai, M. J. Establishment of an animal-bacterial association: recruiting symbiotic vibrios from the environment. *Proc. Natl Acad. Sci. USA* **97**, 10231–10235 (2000).
14. Cohen, S. K. et al. Tracking the cargo of extracellular symbionts into host tissues with correlated electron microscopy and nanoscale secondary ion mass spectrometry imaging. *Cell Microbiol.* **22**, e13177 (2020).
15. Finbow, M. E. & Harrison, M. A. The vacuolar H^+-ATPase: a universal proton pump of eukaryotes. *Biochem. J.* **324**, 697–712 (1997).
16. Nelson, N. & Harvey, W. R. Vacuolar and plasma membrane proton-adenosinetriphosphatases. *Physiol. Rev.* **79**, 361–385 (1999).
17. Shanbhag, S. & Tripathi, S. Epithelial ultrastructure and cellular mechanisms of acid and base transport in the *Drosophila* midgut. *J. Exp. Biol.* **212**, 1731–1744 (2009).
18. Freeman, S. A., Grinstein, S. & Orlowski, J. Determinants, maintenance, and function of organellar pH. *Physiol. Rev.* **103**, 515–606 (2023).
19. Wiriyasermkul, P., Moriyama, S. & Nagamori, S. Membrane transport proteins in melanosomes: Regulation of ions for pigmentation. *Biochim. Biophys. Acta Biomembr.* **1862**, 183318 (2020).
20. Eaton, A. F., Merkulova, M. & Brown, D. The H^+-ATPase (V-ATPase): from proton pump to signaling complex in health and disease. *Am. J. Physiol. Cell Physiol.* **320**, C392–C414 (2021).
21. Li, X. et al. V-Type ATPase mediates airway surface liquid acidification in pig small airway epithelial cells. *Am. J. Respir. Cell Mol. Biol.* **65**, 146–156 (2021).
22. Wong, D., Bach, H., Sun, J., Hmama, Z. & Av-Gay, Y. *Mycobacterium tuberculosis* protein tyrosine phosphatase (PtpA) excludes host vacuolar-H^+-ATPase to inhibit phagosome acidification. *Proc. Natl Acad. Sci. USA* **108**, 19371–19376 (2011).
23. Zhao, J. et al. Molecular basis for the binding and modulation of V-ATPase by a bacterial effector protein. *PLoS Pathog.* **13**, e1006394 (2017).
24. Pu, X. & Qi, B. Lysosomal dysfunction by inactivation of V-ATPase drives innate immune response in *C. elegans*. *Cell Rep.* **43**, 114138 (2024).
25. Allman, E., Johnson, D. & Nehrke, K. Loss of the apical V-ATPase a-subunit VHA-6 prevents acidification of the intestinal lumen during a rhythmic behavior in *C. elegans*. *Am. J. Physiol. Cell Physiol.* **297**, C1071–C1081 (2009).
26. Nepomuceno, D. B. et al. pH control in the midgut of *Aedes aegypti* under different nutritional conditions. *J. Exp. Biol.* **220**, 3355–3362 (2017).
27. Clelland, E. S. & Saleuddin, A. S. Vacuolar-type ATPase in the accessory boring organ of *Nucella lamellosa* (Gmelin) (Mollusca : Gastropoda): role in shell penetration. *Biol. Bull.* **198**, 272–283 (2000).
28. Hill, R. W. et al. Acid secretion by the boring organ of the burrowing giant clam, *Tridacna crocea*. *Biol. Lett.* **14**, 20180047 (2018).
29. McKenzie, E. K. G., Kwan, G. T., Tresguerres, M. & Matthews, P. G. D. A pH-powered mechanochemical engine regulates the buoyancy of *Chaoborus* midge larvae. *Curr. Biol.* **32**, 927–933.e925 (2022).
30. Tresguerres, M., Katz, S. & Rouse, G. W. How to get into bones: proton pump and carbonic anhydrase in *Osedax* boneworms. *Proc. Biol. Sci.* **280**, 20130625 (2013).
31. Armstrong, E. J., Roa, J. N., Stillman, J. H. & Tresguerres, M. Symbiont photosynthesis in giant clams is promoted by V-type H^+-ATPase from host cells. *J. Exp. Biol.* **221**, jeb177220 (2018).
32. Barott, K. L., Thies, A. B. & Tresguerres, M. V-type, H^+-ATPase in the symbiosome membrane is a conserved mechanism for host control of photosynthesis in anthozoan photosymbioses. *R. Soc. Open Sci.* **9**, 211449 (2022).
33. Barott, K. L., Venn, A. A., Perez, S. O., Tambutte, S. & Tresguerres, M. Coral host cells acidify symbiotic algal microenvironment to promote photosynthesis. *Proc. Natl Acad. Sci. USA* **112**, 607–612 (2015).
34. Collins, M. P. & Forgac, M. Regulation and function of V-ATPases in physiology and disease. *Biochim. Biophys. Acta Biomembr.* **1862**, 183341 (2020).
35. Moriano-Gutierrez, S. et al. Critical symbiont signals drive both local and systemic changes in diel and developmental host gene expression. *Proc. Natl Acad. Sci. USA* **116**, 7990–7999 (2019).
36. Perry, S. F. et al. Channels, pumps, and exchangers in the gill and kidney of freshwater fishes: their role in ionic and acid-base regulation. *J. Exp. Zool. A: Comp. Exp. Biol.* **300**, 53–62 (2003).
37. Mashini, A. G., Oakley, C. A., Grossman, A. R., Weis, V. M. & Davy, S. K. Immunolocalization of metabolite transporter proteins in a model cnidarian-dinoflagellate symbiosis. *Appl. Environ. Microbiol.* **88**, e0041222 (2022).
38. Roa, J. N., Munevar, C. L. & Tresguerres, M. Feeding induces translocation of vacuolar proton ATPase and pendrin to the membrane of leopard shark (*Triakis semifasciata*) mitochondrion-rich gill cells. *Comp. Biochem. Physiol. A: Mol. Integr. Physiol.* **174**, 29–37 (2014).
39. De Cian, M. C., Andersen, A. C., Bailly, X. & Lallier, F. H. Expression and localization of carbonic anhydrase and ATPases in the symbiotic tubeworm *Riftia pachyptila*. *J. Exp. Biol.* **206**, 399–409 (2003).
40. Tame, A. et al. mTORC1 regulates phagosome digestion of symbiotic bacteria for intracellular nutritional symbiosis in a deep-sea mussel. *Sci. Adv.* **9**, eadg8364 (2023).
41. Tresguerres, M. Novel and potential physiological roles of vacuolar-type H^+-ATPase in marine organisms. *J. Exp. Biol.* **219**, 2088–2097 (2016).
42. Bertucci, A. et al. Carbonic anhydrases in anthozoan corals—a review. *Bioorg. Med. Chem.* **21**, 1437–1450 (2013).
43. Cardoso, J. C. R. et al. Evolution and diversity of alpha-carbonic anhydrases in the mantle of the Mediterranean mussel (*Mytilus galloprovincialis*). *Sci. Rep.* **9**, 10400 (2019).
44. Leggat, W., Dixon, R., Saleh, S. & Yellowlees, D. A novel carbonic anhydrase from the giant clam *Tridacna gigas* contains two carbonic anhydrase domains. *FEBS J.* **272**, 3297–3305 (2005).
45. Aspatwar, A. et al. Carbonic anhydrases in metazoan model organisms: molecules, mechanisms, and physiology. *Physiol. Rev.* **102**, 1327–1383 (2022).
46. Bidaud-Meynard, A., Nicolle, O., Heck, M., Le Cunff, Y. & Michaux, G. A V_0-ATPase-dependent apical trafficking pathway maintains the polarity of the intestinal absorptive membrane. *Development* **146**, dev174508 (2019).
47. Collaco, A. M., Geibel, P., Lee, B. S., Geibel, J. P. & Ameen, N. A. Functional vacuolar ATPase (V-ATPase) proton pumps traffic to the enterocyte brush border membrane and require CFTR. *Am. J. Physiol. Cell Physiol.* **305**, C981–C996 (2013).
48. Levic, D. S. & Bagnat, M. Self-organization of apical membrane protein sorting in epithelial cells. *FEBS J.* **289**, 659–670 (2022).
49. Sun-Wada, G. H. & Wada, Y. Exploring the link between vacuolar-type proton ATPase and epithelial cell polarity. *Biol. Pharm. Bull.* **45**, 1419–1425 (2022).
50. Wax, M. B. et al. Vacuolar H^+-ATPase in ocular ciliary epithelium. *Proc. Natl Acad. Sci. USA* **94**, 6752–6757 (1997).
51. Bowman, E. J., Graham, L. A., Stevens, T. H. & Bowman, B. J. The bafilomycin/concanamycin binding site in subunit c of the V-ATPases from *Neurospora crassa* and *Saccharomyces cerevisiae*. *J. Biol. Chem.* **279**, 33131–33138 (2004).
52. Yee, D. P. et al. The V-type ATPase enhances photosynthesis in marine phytoplankton and further links phagocytosis to symbiogenesis. *Curr. Biol.* **33**, 2541–2547 e2545 (2023).
53. Drose, S. & Altendorf, K. Bafilomycins and concanamycins as inhibitors of V-ATPases and P-ATPases. *J. Exp. Biol.* **200**, 1–8 (1997).

54. Drose, S. et al. Inhibitory effect of modified bafilomycins and concanamycins on P- and V-type adenosine triphosphatases. *Biochemistry* **32**, 3902–3906 (1993).
55. Huss, M. et al. Concanamycin A, the specific inhibitor of V-ATPases, binds to the V_o subunit c. *J. Biol. Chem.* **277**, 40544–40548 (2002).
56. Oot, R. A., Yao, Y., Manolson, M. F. & Wilkens, S. Purification of active human vacuolar H^+-ATPase in native lipid-containing nanodiscs. *J. Biol. Chem.* **297**, 100964 (2021).
57. Foster, J. S. & McFall-Ngai, M. J. Induction of apoptosis by cooperative bacteria in the morphogenesis of host epithelial tissues. *Dev. Genes Evol.* **208**, 295–303 (1998).
58. Koropatnick, T. A., Kimbell, J. R. & McFall-Ngai, M. J. Responses of host hemocytes during the initiation of the squid-vibrio symbiosis. *Biol. Bull.* **212**, 29–39 (2007).
59. Nyholm, S. V. & McFall-Ngai, M. J. Dominance of *Vibrio fischeri* in secreted mucus outside the light organ of *Euprymna scolopes*: the first site of symbiont specificity. *Appl. Environ. Microbiol.* **69**, 3932–3937 (2003).
60. Nishiguchi, M. et al. Increase in secretion of glial cell line-derived neurotrophic factor from glial cell lines by inhibitors of vacuolar ATPase. *Neurochem. Int.* **42**, 493–498 (2003).
61. Gundlach, K. A. et al. Ciliated epithelia are key elements in the recruitment of bacterial partners in the squid-vibrio symbiosis. *Front. Cell Dev. Biol.* **10**, 974213 (2022).
62. Aschtgen, M. S. et al. Rotation of *Vibrio fischeri* flagella produces outer membrane vesicles that induce host development. *J. Bacteriol.* **198**, 2156–2165 (2016).
63. Koehler, S. et al. The model squid-vibrio symbiosis provides a window into the impact of strain- and species-level differences during the initial stages of symbiont engagement. *Environ. Microbiol.* https://doi.org/10.1111/1462-2920.14392 (2018).
64. Lee, K. & Ruby, E. G. Symbiotic role of the viable but nonculturable state of *Vibrio fischeri* in Hawaiian coastal seawater. *Appl. Environ. Microbiol.* **61**, 278–283 (1995).
65. Boettcher, K. J. & Ruby, E. G. Depressed light emission by symbiotic *Vibrio fischeri* of the sepiolid squid *Euprymna scolopes*. *J. Bacteriol.* **172**, 3701–3706 (1990).
66. Belcaid, M. et al. Symbiotic organs shaped by distinct modes of genome evolution in cephalopods. *Proc. Natl Acad. Sci. USA* **116**, 3030–3035 (2019).
67. Altschul, S. F., Gish, W., Miller, W., Myers, E. W. & Lipman, D. J. Basic local alignment search tool. *J. Mol. Biol.* **215**, 403–410 (1990).
68. Katoh, K. & Standley, D. M. MAFFT multiple sequence alignment software version 7: improvements in performance and usability. *Mol. Biol. Evol.* **30**, 772–780 (2013).
69. Minh, B. Q. et al. IQ-TREE 2: New models and efficient methods for phylogenetic inference in the genomic era. *Mol. Biol. Evol.* **37**, 1530–1534 (2020).
70. Letunic, I. & Bork, P. Interactive Tree Of Life (iTOL) v5: an online tool for phylogenetic tree display and annotation. *Nucleic Acids Res.* **49**, W293–W296 (2021).
71. Jumper, J. et al. Highly accurate protein structure prediction with AlphaFold. *Nature* **596**, 583–589 (2021).
72. Heath-Heckman, E. A. et al. Bacterial bioluminescence regulates expression of a host cryptochrome gene in the squid-vibrio symbiosis. *mBio* **4**, e00167–13 (2013).
73. Troll, J. V. et al. Taming the symbiont for coexistence: a host PGRP neutralizes a bacterial symbiont toxin. *Environ. Microbiol.* **12**, 2190–2203 (2010).
74. Barott, K. & Tresguerres, M. Immunolocalization of proteins in corals the V-type H^+- ATPase proton pump. *Bio-Protoc.* **5**, 1–10 (2015).
75. Mastronarde, D. N. Automated electron microscope tomography using robust prediction of specimen movements. *J. Struct. Biol.* **152**, 36–51 (2005).
76. Kremer, J. R., Mastronarde, D. N. & McIntosh, J. R. Computer visualization of three-dimensional image data using IMOD. *J. Struct. Biol.* **116**, 71–76 (1996).
77. Mastronarde, D. N. Correction for non-perpendicularity of beam and tilt axis in tomographic reconstructions with the IMOD package. *J. Microsc.* **230**, 212–217 (2008).
78. Schindelin, J. et al. Fiji: an open-source platform for biological-image analysis. *Nat. Methods* **9**, 676–682 (2012).
79. Schwartzman, J. A. et al. The chemistry of negotiation: rhythmic, glycan-driven acidification in a symbiotic conversation. *Proc. Natl Acad. Sci. USA* **112**, 566–571 (2015).
80. Christensen, D. G. & Visick, K. L. *Vibrio fischeri*: Laboratory cultivation, storage, and common phenotypic assays. *Curr. Protoc. Microbiol.* **57**, e103 (2020).
81. Chung, Y., Rabe-Hesketh, S., Dorie, V., Gelman, A. & Liu, J. A nondegenerate penalized likelihood estimator for variance parameters in multilevel models. *Psychometrika* **78**, 685–709 (2013).
82. Hothorn, T., Bretz, F. & Westfall, P. Simultaneous inference in general parametric models. *Biom. J.* **50**, 346–363 (2008).
83. Rogers, T. F. et al. Gene modelling and annotation for the Hawaiian bobtail squid, *Euprymna scolopes*. *Sci. Data* **11**, 40 (2024).

Acknowledgements

The authors thank R. Scarborough, A. Castro, and N. Ranieri for the maintenance of the squid husbandry facility, and members of the McFall-Ngai and Ruby laboratories for comments on the manuscript. This work was funded by National Institutes of Health grants R37-AI50661 to M.M.-N. and E.G.R. and R01-GM135254 to E.G.R. and M.M.-N. J.W.V. and A.B.T. were funded by National Science Foundation Graduate Research Fellowships (GRFP 1842402 and GRFP 2019271478, respectively). A.B.T. was also supported by an Achievement Rewards for College Scientists (ARCS) Fellowship.

Author contributions

Conceptualization: J.W.V., M.M.-N., M.T., E.G.R. Methodology: J.W.V., M.M.-N., M.T., E.G.R., S.K., A.B.T., A.C.H., M.L., G.Y.C., J.K. Investigation: All authors. Visualization: A.C.H., J.V.W., M.M.-N., M.T., E.G.R., S.K., A.B.T., M.L., V.A.-M. Supervision: M.M.-N., M.T., E.G.R. Writing- original draft: M.M.-N, A.C.H., J.W.V., M.T., E.G.R. Writing- review and editing: All authors.

Competing interests

The authors declare no competing interests.

Additional information

Supplementary information The online version contains supplementary material available at https://doi.org/10.1038/s42003-024-07348-2.

Correspondence and requests for materials should be addressed to Margaret J. McFall-Ngai.

Peer review information *Communications Biology* thanks Manuel Kleiner and the other, anonymous, reviewers for their contribution to the peer review of this work. Primary Handling Editor: Tobias Goris.